



**HAL**  
open science

## Examination of nuclear chirality with a magnetic moment measurement of the $I = 9$ isomeric state in $^{128}\text{Cs}$

E. Grodner, M. Kowalczyk, M. Kisieliński, J. Srebrny, L. Próchniak, Ch. Droste, S. Rohoziński, Q. Chen, M. Ionescu-Bujor, C. Ur, et al.

### ► To cite this version:

E. Grodner, M. Kowalczyk, M. Kisieliński, J. Srebrny, L. Próchniak, et al.. Examination of nuclear chirality with a magnetic moment measurement of the  $I = 9$  isomeric state in  $^{128}\text{Cs}$ . *Physical Review C*, 2022, 106 (1), pp.014318. 10.1103/PhysRevC.106.014318 . hal-03763793

**HAL Id: hal-03763793**

**<https://hal.science/hal-03763793>**

Submitted on 3 Nov 2022

**HAL** is a multi-disciplinary open access archive for the deposit and dissemination of scientific research documents, whether they are published or not. The documents may come from teaching and research institutions in France or abroad, or from public or private research centers.

L'archive ouverte pluridisciplinaire **HAL**, est destinée au dépôt et à la diffusion de documents scientifiques de niveau recherche, publiés ou non, émanant des établissements d'enseignement et de recherche français ou étrangers, des laboratoires publics ou privés.

# To be or not to be chiral – the magnetic moment measurement of the $I = 9$ isomeric state in $^{128}\text{Cs}$

E. Grodner,<sup>1</sup> M. Kowalczyk,<sup>2</sup> M. Kisieliński,<sup>2</sup> J. Srebrny,<sup>2</sup> L. Próchniak,<sup>2</sup> Ch. Droste,<sup>3</sup> S. G. Rohoziński<sup>†\*</sup>,<sup>3</sup> Q. B. Chen,<sup>4</sup> M. Ionescu-Bujor,<sup>5</sup> C. A. Ur,<sup>6</sup> F. Recchia,<sup>6</sup> J. Meng,<sup>7,8,9</sup> S. Zhang,<sup>7</sup> P. W. Zhao,<sup>7</sup> G. Georgiev,<sup>10</sup> R. Lozeva,<sup>10</sup> E. Fiori,<sup>10</sup> S. Aydin,<sup>11</sup> and A. Nałęcz-Jawecki<sup>1</sup>

<sup>1</sup>*National Centre for Nuclear Research, 05-540 Świerk, Poland*

<sup>2</sup>*Heavy Ion Laboratory, University of Warsaw, 02-093 Warsaw, Poland*

<sup>3</sup>*Faculty of Physics, University of Warsaw, 02-093 Warsaw, Poland*

<sup>4</sup>*Department of Physics, East China Normal University, Shanghai 200241, China*

<sup>5</sup>*Horia Hulubei National Institute for Physics and Nuclear Engineering, 077125 Bucharest, Romania*

<sup>6</sup>*Instituto Nazionale di Fisica Nucleare, I-35131 Padova, Italy*

<sup>7</sup>*State Key Laboratory of Nuclear Physics and Technology,*

*School of Physics, Peking University, Beijing 100871, China*

<sup>8</sup>*School of Physics, Beihang University, Beijing 102206, China*

<sup>9</sup>*Yukawa Institute for Theoretical Physics, Kyoto University, Kyoto 606-8502, Japan*

<sup>10</sup>*IJCLab, CNRS/IN2P3; Université Paris-Saclay, 91405 Orsay, France*

<sup>11</sup>*Department of Natural and Mathematical Sciences,*

*Faculty of Engineering, Tarsus University, 33480, Mersin, Turkey*

The  $g$  factor of the isomeric  $I = 9^+$  bandhead of the yrast states in  $^{128}\text{Cs}$  is obtained from the Time Differential Perturbed Angular Distribution measurement performed with the electromagnet at IPN Orsay. External magnetic field of 2.146 T at the target position has been attained with GAMPE reaction chamber surrounded by four HPGe detectors from which two were of LEPS type. The results are in accordance with  $\pi h_{11/2} \otimes \nu h_{11/2}^{-1}$   $I = 9^+$  bandhead assignment and are discussed in the context of chiral interpretation of the  $^{128}\text{Cs}$  nucleus as a composition of the odd proton, odd neutron and even-even core with their angular momentum vectors. The obtained  $g$ -factor value has been compared with predictions of particle-rotor model. The experimental  $g$  factor corresponds to the non-chiral geometry of the isomeric bandhead. This observation indicates the existence of the chiral critical frequency in  $^{128}\text{Cs}$  and may explain the absence of the chiral doublet members for  $I < 13\hbar$ .

December 24, 2021

## I. INTRODUCTION

The  $^{128}\text{Cs}$  nucleus studied in this paper belongs to a group of nuclei around  $A \approx 130$  in which the phenomenon of nuclear chirality [1] has been reported through the observation of chiral doublet states [2] and a specific selection rules for the gamma transitions between these states [3–6].

The chiral partner bands in  $^{128}\text{Cs}$  nucleus are described as coupling of three components: an even-even core with angular momentum  $j_R$  and two odd nucleons in  $\pi h_{11/2} \otimes \nu h_{11/2}^{-1}$  configuration with angular momentum  $j_p$  and  $j_n$ , respectively. The reported observables serve as an indirect sign of the chiral geometry formed in  $^{128}\text{Cs}$  nucleus where the three angular momentum vectors span the three dimensional space.

In the ideal geometry the  $j_R$ ,  $j_p$ , and  $j_n$  vectors are mutually perpendicular and build either right- or left-handed reference frame corresponding to left  $|L\rangle$  and right-handed  $|R\rangle$  intrinsic nuclear states. The mechanism of the spontaneous chiral symmetry breaking in nuclear

system occurs when an excited nucleus cools down and at some point chooses spontaneously one of the two intrinsic states. The nucleus does not stay in the chosen intrinsic configuration since it is not its eigenstate. Tunneling between  $|L\rangle$  and  $|R\rangle$  configurations takes place with period much shorter than the time required for the gamma quantum emission to occur from the excited states of the nucleus. This is why the intrinsic states with specified handedness cannot directly be observed in gamma spectroscopy experiments. Instead of the  $|L\rangle$  and  $|R\rangle$  intrinsic configurations their projections onto the eigenstates of the nucleus, i.e. chiral doublets, are seen through observation of the emitted gamma rays. Therefore, the handedness of the three angular momentum vectors is fundamentally hidden for nuclear spectroscopy investigations where chiral doublets and other associated observables indicate the existence of spontaneous chiral symmetry breaking.

Even though the handedness cannot be observed directly, the magnetic dipole moment allows to study the nuclear chirality regardless of the handedness in which the nucleus actually is. It turns out that the value of the magnetic dipole moment and the corresponding value of the  $g$  factor is a function of the geometry formed by the three angular momentum vectors through their scalar

---

\*deceased

products. These products are symmetric with respect to handedness giving non-zero values in the symmetric eigenstates with mixed handedness. Therefore, the value of the  $g$  factor may give information whether the three angular momentum vectors span a three-dimensional space (chiral configuration) or lie in one plane (planar or non-chiral configuration) regardless of the handedness in which the intrinsic dynamical state actually is.

In this paper, the  $g$ -factor value of the isomeric  $I = 9^+$  bandhead of the yrast states in  $^{128}\text{Cs}$  has been measured with classical Time Dependent Perturbed Angular Distribution (TDPAD) method. It is the lowest lying state in the rotational yrast band being one of the chiral partners built on  $\pi h_{11/2} \otimes \nu h_{11/2}^{-1}$  configuration. The chiral character of the partner bands in  $^{128}\text{Cs}$  has been observed in states with significant nuclear rotation corresponding to spins higher than  $13\hbar$  [3]. With decreasing nuclear rotation the yrast band is not observed leaving room for two hypotheses, one of which assumes that the nuclear chirality persists at low rotational frequency although low spins of the yrast band are not fed by fusion reaction mechanism. In such a case the  $g$ -factor value of the bandhead should correspond to a chiral geometry of the three component system. The other hypothesis states that there is a phase transition suppressing the chiral geometry at low rotational frequency. This may happen below the chiral critical frequency [7] predicted by tilted axis cranking model. Existence of this critical frequency may prevent the chiral geometry to develop in energy favored nuclear states. Thus a non-chiral or planar character of the bandhead is expected. This article details the experimental as well as the theoretical methods for the magnetic moment measurement and its interpretation, the results of which were briefly published in [8]. The principle of the measurement and methods of the data analysis are described in chapters II and III. Chapter IV and V contains analytical considerations of the magnetic moment as formed by single coupling schemes of two or of three angular momentum vectors, while chapters VI and VII presents detailed calculation and interpretation in the frame of many-particle-many-hole particle rotor model.

## II. EXPERIMENTAL SETUP

The  $^{128}\text{Cs}$  nucleus has been produced in  $^{122}\text{Sn}(^{10}\text{B}, 4n)^{128}\text{Cs}$  fusion-evaporation reaction at 55 MeV beam energy. Pulsed  $^{10}\text{B}$  beam with 1 ns bursts and 400 ns repetition period has been developed by the Tandem accelerator at IPN Orsay. Single gamma quanta were registered by two LEPS detectors placed at  $\pm 45$  degrees with respect to beam axis. The decay of the  $I = 9^+$  isomeric state has been studied using off-beam sorted coincidences of gamma quanta registered between beam pulses [9]. Relevant part of the level scheme is shown in Fig. 1 where 14 prompt gamma transitions follow the  $I = 9^+$  isomeric state decay.

These transitions were subject of the TDPAD mea-

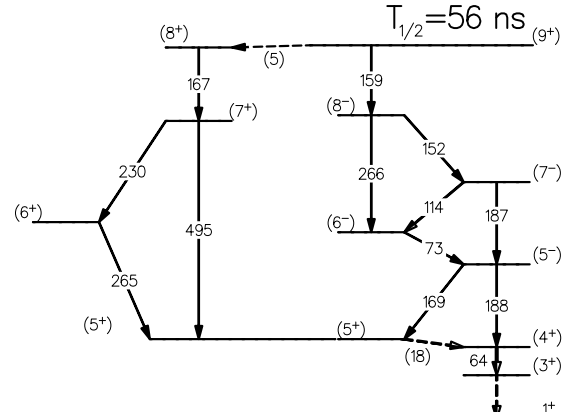


Figure 1: Relevant part of the level scheme of  $^{128}\text{Cs}$  obtained in Ref. [9]. Decay of the isomeric state reconstructed from coincidences collected between beam pulses and from prompt-delayed gamma coincidences. The two transitions represented by dashed lines, 18 keV and 5 keV, are below the sensitivity threshold of the experiment due to high electron-conversion decay mode.

surement with external magnetic field produced by an electromagnet at IPN Orsay. Interaction of the external magnetic field and the magnetic moment associated with a nuclear state leads to precession of the nuclear angular momentum vector. To get the  $g$ -factor value with high precession at least half circumvolution of the nuclear spin should occur in the period of the isomeric level lifetime. The Larmor frequency of precession  $\omega_L = -g\mathbf{B}\mu_N/\hbar$  is proportional to the nuclear  $g$  factor and the external magnetic field. The half-life of the isomeric state  $T_{1/2} = 56 \text{ ns}$  [9] together with theoretical estimates of its  $g$  factor  $g \approx 0.5$  [10] gave the required magnetic field to be  $B \approx 2 \text{ T}$  for a half circumvolution within 50 ns period. The magnetic field of around 0.7 T attainable at the electromagnet was magnified with help of the GAMPIPE reaction chamber of NIPNE (National Institute for Physics and Nuclear Engineering, Romania), see Fig. 2.

The GAMPIPE chamber equipped with cone-shaped iron poles allowed to focus the magnetic field that reached 2.146 T in the target position. In Fig. 2 the uniformity of the magnetic field is presented as a plot of the B-field vs. horizontal distance from the center of the chamber. One can see that the magnetic field changes about 1.2% within the  $\pm 5 \text{ mm}$  distance being the target diameter. This change had to be taken into account since the projectiles were deflected from the center point of the target by the applied magnetic field. The final position of the  $1 \text{ mm}^2$  beam spot in the target plane was determined by burning a beam fleck in a paper layer placed instead of the target foil (cf. Fig. 2). This allows precise measurement of the magnetic field  $B = 2.146 \text{ T}$  at the beam spot before and after the experiment. Fig. 3 shows the geometry of the experimental setup.

The  $^{122}\text{Sn}(^{10}\text{B}, 4n)^{128}\text{Cs}$  reaction populated the aligned states of  $^{128}\text{Cs}$  recoils that stopped in the Sn

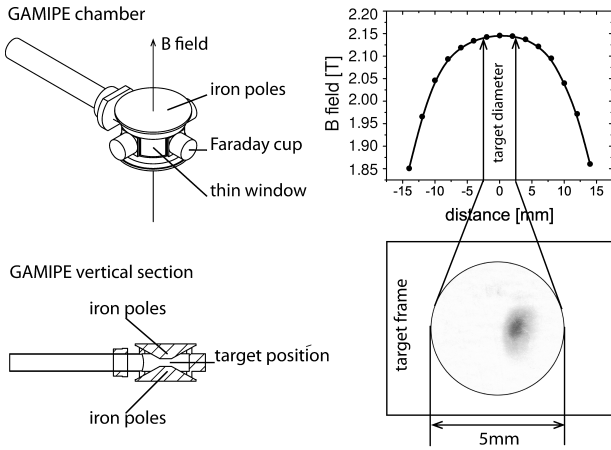


Figure 2: GAMPIPE reaction chamber, B field uniformity, beam spot.

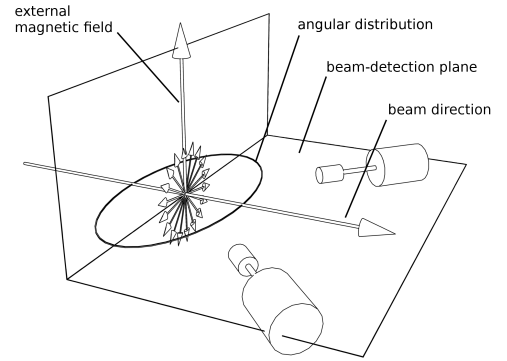


Figure 4: Experimental setup arrangement.

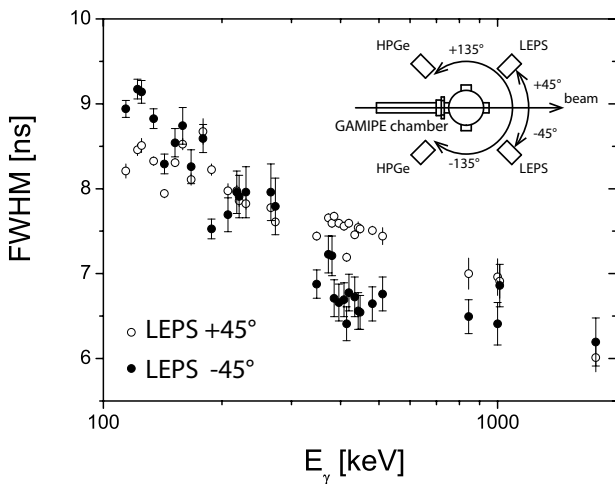


Figure 3: Experimental geometry, timing resolution.

target of  $22 \text{ mg/cm}^2$  thickness. Small initial velocity  $v \approx 0.01c$  [3] as well as short stopping time  $t_{\text{stop}} \approx 1 \text{ ps}$  of recoils ensures the decay of the isomeric state to happen mostly from  $^{128}\text{Cs}$  nuclei at rest. Therefore, both the spin alignment and the distribution of the gamma radiation had a mirror symmetry with respect to the plane perpendicular to the beam direction, which is shown schematically in Fig. 4. Precession of the angular distribution with a frequency  $\omega_L$  was observed by an intensity modulation which frequency was twice higher as a result of the mirror symmetry. The modulation period of around  $50 \text{ ns}$  was registered by two low energy photon spectrometer (LEPS) of Laboratori Nazionali di Legnaro. As shown in Fig. 4, the two LEPS detectors were placed at angles  $\pm 45^\circ$  with respect to the beam axis forming a beam-detection plane and the magnetic field perpendicular to it.

The excellent time resolution of LEPS detectors vs.  $\gamma$ -quanta energy, shown in Fig. 3, is gained at the expense

of registration efficiency of high-energy electromagnetic radiation. Therefore two other Ge-spectrometers – standard HPGe (High Purity Ge) detectors with beryllium window and 35% relative efficiency – were placed at angles  $\pm 135^\circ$  with respect to the beam axis in order to increase the registration efficiency for high-energy gammas. Neither of the four Ge detectors was equipped with ACS (Anti Compton Shield) shielding. Fig. 3 shows that time resolution of LEPS detectors in the present experiment is around  $8 \text{ ns}$  for  $E_\gamma \approx 120 \text{ keV}$  and drops to around  $6 \text{ ns}$  for  $E_\gamma \approx 1700 \text{ keV}$ . Electronic appliances i.e. spectroscopic amplifiers, TAC (Time-to-Amplitude Converter), CFD (Constant Fraction Discriminator), TFA (Timing Filter Amplifier) and two HPGe detectors with 35% efficiency were delivered by Heavy Ion Laboratory of the University of Warsaw while events signals readout in a single gamma mode was done with Orsay data acquisition system.

For a single gamma quantum information on its energy (taken from the spectroscopic amplifiers) and registration time with respect to beam pulse (taken from TAC) were collected. Each Ge detector had the start socket of the TAC connected with the logic output signal from the associated CFD, whereas the stop socket of the TAC was connected with the signal from TANDEM accelerator.

Single gamma quanta were collected during 5 days of the beam time. The energy gated time spectra for the  $g$ -factor evaluation were then constructed in off-beam mode using HIL (Heavy Ion Laboratory) sorting software.

### III. DATA ANALYSIS AND RESULTS

The  $I = 9^+$  isomeric state decays via 167 and 159 keV transitions which are followed by emission of another 12 gamma quanta [9]. Modulated intensity has been observed for all transitions below the isomer except 18 keV and 5 keV lines which are below the sensitivity threshold of the experiment due to high electron-conversion

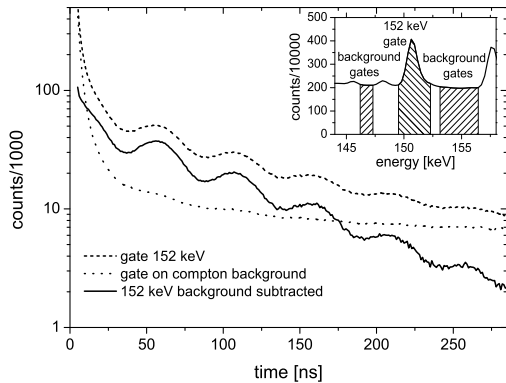


Figure 5: Background subtraction from the time spectrum of 152 keV peak.

decay mode. The intensity modulation of the Compton background can mimic the modulation effect for the given transition. Therefore, background subtracted time spectra were produced where a time spectrum gated on gamma peak was subtracted by a time spectrum gated on the background.

Fig. 5 illustrates the time spectrum gated on the  $E = 152$  keV peak with and without background subtraction together with the time spectrum of the Compton background. The modulated intensity follows a straight line in the logarithmic scale indicating proper background subtraction. Background subtracted oscillation spectra have been found for 11 gamma lines associated with the isomeric state decay.

Rotating angular distribution inherits the symmetry of the rotating spin alignment giving intensity modulations of opposite phase observed by the LEPS detectors placed at the right angle in the beam-detection plane. All oscillation spectra observed in the present experiment are shown in Fig. 6 where the spectra have been normalized by multiplying the  $-45^\circ$  LEPS spectra by a factor of 2.4.

One can see that oscillation of 114 keV transition in the first 70 ns after the beam pulse is disturbed by an overlapping unidentified 115 keV peak. The 115 keV line is observed in coincidence with 122 keV gamma which presents much shorter half-life than 56 ns half-life of the  $I = 9^+$  isomeric state. Therefore, the analysis of the 114 keV oscillations has been performed for gammas registered after the 70 ns decay of the overlapping transition. Rotation of the angular distribution leads to the modulation of the gamma intensity observed by a detector in the beam detection plane according to the formula

$$I(\theta, t) = I_0 \cdot e^{-t/\tau} [1 + \alpha_2(t)Q_2A_2P_2(\cos(\theta - \omega_L t)) + \alpha_4(t)Q_4A_4P_4(\cos(\theta - \omega_L t))], \quad (1)$$

where  $A_2$ ,  $A_4$  are the gamma angular distribution coefficients,  $Q$ ,  $\alpha(t)$  the attenuation factors due to the finite detector size and time dependent spin alignment,  $\tau$  the

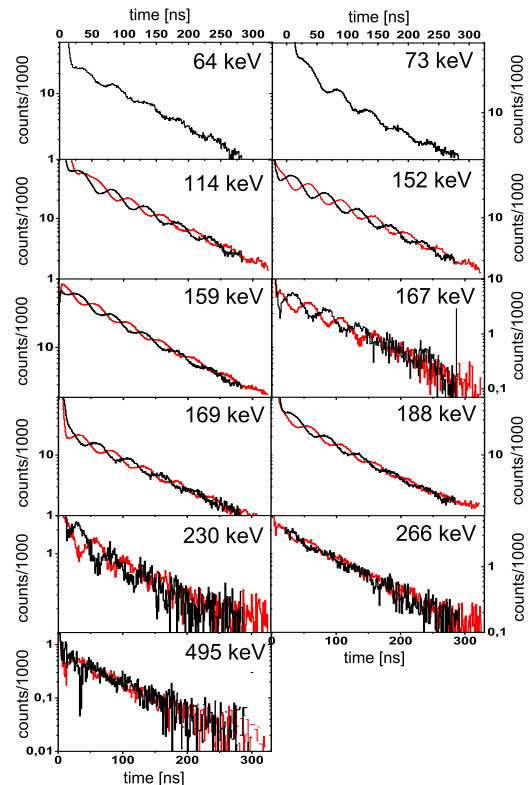


Figure 6: Intensity oscillation spectra registered by LEPS detectors. Dotted line shows the intensity registered at  $+45^\circ$  with respect to beam axis while solid line the intensity seen at  $-45^\circ$ . The intensity curves have been normalized by multiplying the  $-45^\circ$  spectrum by factor of 2.4.

$I = 9^+$  isomeric state lifetime, and  $\omega_L$  being the Larmor frequency of precession. Only even Legendre polynomials  $P_2$  and  $P_4$  are present in the formula (1) as a result of the mirror symmetry of the initial gamma angular distribution. With an assumption of identical detector properties one gets the same  $Q$  attenuation factors for both detectors. This allows to get precise value of the Larmor frequency by constructing a modulation ratio spectra. A modulation ratio of the detectors placed at the right angle is defined as

$$R(t) = \frac{I(-45^\circ, t) - I(+45^\circ, t)}{I(-45^\circ, t) + I(+45^\circ, t)}, \quad (2)$$

where the numerator becomes

$$\begin{aligned} & I(-45^\circ, t) - I(+45^\circ, t) \\ &= I_0 \cdot e^{-t/\tau} \left[ \frac{3}{2} \alpha_2(t) Q_2 A_2 \right. \\ & \quad \left. + \frac{10}{16} \alpha_4(t) Q_4 A_4 \right] \cos(2(-45^\circ - \omega_L t)), \end{aligned} \quad (3)$$

while the denominator simplifies to

$$I(-45^\circ, t) + I(+45^\circ, t)$$

$$= I_0 \cdot e^{-t/\tau} \left[ 2 + \frac{1}{2} \alpha_2(t) Q_2 A_2 + \frac{1}{16} \alpha_4(t) Q_4 A_4 (35 \cos^2(2(-45^\circ - \omega_L t)) - 13) \right]. \quad (4)$$

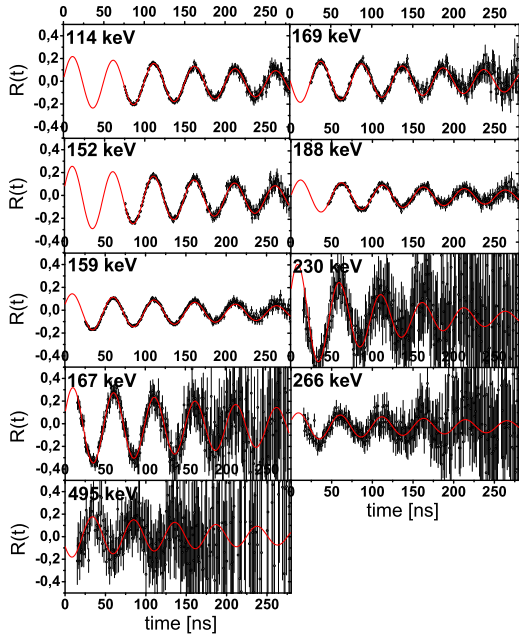


Figure 7: Observed oscillating ratios  $R(t)$ .

For the assumption of identical detectors and small  $A_4$  coefficients, one gets approximate modulation ratio of the form

$$R(t) \approx \frac{-3\alpha_2(t)Q_2A_2 \sin(2\omega_L t - \phi)}{4 + \alpha_2(t)Q_2A_2}, \quad (5)$$

where additional parameter the phase  $\phi$  has been introduced to account for possible timing offsets of the detectors. Fig. 7 shows modulation spectra constructed by means of Eq. (2) with least-squares fits of formula (5) shown as solid lines. The approximate modulation formula describes the experimental data very well indicating that the assumption of small  $A_4$  coefficients and identical detectors is a sufficient approximation for the Larmor frequency to be measured. However, this approximation may not be correct for gamma angular distribution coefficients determination that may be sensitive to spectra normalization and summation.

One can see in Fig. 7 an attenuated oscillation amplitudes, which may come from the hyperfine interaction between the nuclear magnetic moment of Cs recoils and the magnetic moments of the electronic shells in Sn target causing spin deorientation effect. The relaxation time of the spin deorientation and the corresponding oscillations attenuation is around  $\tau_{\text{rel}} \approx 300$  ns. The deorientation

effect has been included in the fitted formula by the spin alignment coefficients  $\alpha(t)$  taken as exponential function of time  $\alpha_2(t) = \alpha_2 \exp(-t/\tau_{\text{rel}})$ . Thus the final approximate function for the observed modulation ratio becomes

$$R(t) \approx \frac{-3 \exp(-t/\tau_{\text{rel}}) A \sin(2\omega_L t - \phi)}{4 + A \exp(-t/\tau_{\text{rel}})}, \quad (6)$$

where  $A = \alpha_2 Q_2 A_2$  has been assigned as the value related to initial modulation amplitude.

Table I: Parameters of the oscillation function given by the Eq. (6) resulted from the fitting procedure.

$E_\gamma$ [keV]	$A$	$\omega_L$ [ $10^9 \text{s}^{-1}$ ]	$\phi$ [ $^\circ$ ]	$\tau_{\text{rel}}$ [ns]
114	-0.243(9)	0.0625(1)	$7.9 \pm 2.0$	$334 \pm 34$
152	-0.296(4)	0.0622(1)	$19.7 \pm 0.7$	$279 \pm 12$
159	-0.172(3)	0.0620(1)	$23.6 \pm 1.0$	$255 \pm 15$
167	-0.35(2)	0.0618(4)	$20.7 \pm 3.4$	$360 \pm 101$
169	+0.193(6)	0.0631(2)	$-3.7 \pm 1.6$	$373 \pm 53$
188	-0.153(7)	0.0625(2)	$3.3 \pm 2.5$	$277 \pm 36$
230	-0.51(7)	0.062(1)	$25.6 \pm 9.5$	$123 \pm 31$
266	-0.12(1)	0.061(2)	$24.2 \pm 14.7$	$300^a$
495	+0.19(3)	0.062(2)	$28.1 \pm 23.3$	$300^a$

<sup>a</sup>fixed during fitting.

The  $A$ ,  $\tau_{\text{rel}}$ ,  $\omega_L$ , and  $\phi$  parameters were kept free for the least-squares fits of the formula (6) giving the results listed in Table I. One can see that the Larmor frequency  $\omega_L$  in all of the oscillation functions is nearly the same. This suggests that the intensity ratios  $R(t)$  come from fast  $\gamma$ -transitions below the  $I = 9^+$  isomer. All excited states above the isomer belong to collective bands with picosecond lifetimes [3] and do not contribute to the modulation of the intensity ratio. This is particularly important information, since the experiment discussed here is a  $\gamma$ -distribution and not the  $\gamma$ -correlation measurement. The oscillation frequency observed in all transitions can therefore be attributed to the  $g$  factor of the  $I = 9^+$  bandhead, leading to precise values of the  $g$  factor  $g = 0.59(1)$  as well as of the deorientation relaxation time  $\tau = 3.43(8) \cdot 10^{-7} \text{s}$  [8]. The obtained  $g$ -factor value is about 20% larger than expected theoretically in frame of CPHC calculations with  $\gamma$ -rigid as well as  $\gamma$ -soft core [10, 11].

#### IV. $\pi h_{11/2} \otimes \nu h_{11/2}^{-1} I = 9^+$ BANDHEAD CONFIGURATION

The obtained value of the  $g$  factor for  $I = 9^+$  bandhead allows to verify whether the total angular momentum vector of  $9^+$  bandhead is build chiefly by the two angular momentum vectors of the odd  $\pi h_{11/2} \otimes \nu h_{11/2}^{-1}$  nucleons or a third component coming from significant even-even core rotation is required to reproduce the value observed experimentally.

Table II: Estimation of the  $g$ -factor value of  $I = 9^+$  in  $^{128}\text{Cs}$  based on pure theoretical calculations (first row) and on experimental data taken from neighboring nuclei (second and third row) with comparison to experimentally obtained  $g$  factor. Column 1: orbitals from which the input values are taken. Column 2: Isotopes from which the input data are taken. Column 3 and 4: values of single particle proton and neutron  $g$  factors being the input data [12]. Column 5 and 6: values of spin gyromagnetic factors of proton and of neutron calculated from proton and neutron single-particle  $g$  factors. Column 7 and 8: Single particle  $g$  factor for proton and neutron expected in  $h_{11/2}$  orbital from corresponding spin gyromagnetic factors. Column 9: values of the  $g$  factor in  $\pi h_{11/2} \otimes \nu^{-1} h_{11/2}$   $I = 9^+$  state of  $^{128}\text{Cs}$  expected for two component model (no core rotation). Column 10: value of the  $g$  factor obtained experimentally.

orbital	isotope	$g^j$ proton	$g^j$ neutron	$g^s$ proton	$g^s$ neutron	$g_p$	$g_n$	$g$	$g_{\text{experiment}}$
$h_{11/2}$ theoretical	$^{128}\text{Cs}$	1.21	-0.21	3.31	-2.31	$1.21^a$	$-0.21^a$	$0.50^a$	0.59(1) (experimental)
$h_{11/2}$	$^{129}\text{Cs}(\text{proton})/^{129}\text{Xe}(\text{neutron})$	1.191(18)	-0.1619(2)	3.10(2)	-1.781(2)	1.191(18)	-0.1619(2)	0.515(9)	
$s_{1/2}$	$^{127}\text{Cs}(\text{proton})/^{129}\text{Xe}(\text{neutron})$	2.98(2)	-1.555953(15)	2.98(2)	-1.555953(15)	1.1802(15)	-0.1414502(15)	0.519(2)	

<sup>a</sup>gyromagnetic factors of proton  $g_p$  and neutron  $g_n$  taken from theoretical estimates [14–16].

In case where only two angular momentum vectors of the two odd nucleons contribute to the total spin of the isomeric state (no core rotation) there is only one coupling scheme giving the required total angular momentum  $J = 9\hbar$ . The  $g$  factor of such two-component state can be calculated using the additivity formula [13]

$$g = \frac{1}{2J(J+1)} \left\{ g_p [J(J+1) + j_p(j_p+1) - j_n(j_n+1)] + g_n [J(J+1) - j_p(j_p+1) + j_n(j_n+1)] \right\}, \quad (7)$$

where  $g_p$  and  $g_n$  are  $g$  factors of the odd proton and odd-neutron, respectively.

For the  $\pi h_{11/2} \otimes \nu h_{11/2}^{-1}$  configuration, the angular momentum of the proton  $j_p$  and the neutron  $j_n$  equals to  $11/2\hbar$  and the above formula simplifies to

$$g = \frac{1}{2}(g_p + g_n). \quad (8)$$

To find the value of  $g_p$  and  $g_n$  one can use theoretical estimations [14–16] or adopt it from experimental data of magnetic moments measured in the neighboring single-odd nuclei. For a single nucleon occupying the  $j = l \pm s$  orbital its  $g$ -factor value can be written as

$$g^j = \frac{(2j-1)g^l + g^s}{2j}, \quad \text{for } j = l + \frac{1}{2}, \quad (9)$$

$$g^j = \frac{(2j+3)g^l - g^s}{2(j+1)}, \quad \text{for } j = l - \frac{1}{2}. \quad (10)$$

These two equations allow to express the  $g_p$  and  $g_n$  values for any nuclear orbital provided that the spin-gyromagnetic factors  $g^s$  of these particles are known, or

in opposite, for the known  $g$ -factor value of specified orbital it is possible to get the  $g^s$  values. By taking the orbital gyromagnetic factor  $g^l = 1$  for the proton and  $g^l = 0$  for the neutron together with the measured magnetic moments of states in neighboring nuclei, one can get an estimation of the associated  $g^s$  values.

The  $^{128}\text{Cs}$  is a doubly-odd nucleus with 73 neutrons and 55 protons. In a single-odd neighbors, one can get either the features of the proton states from  $^{129}\text{Cs}$  data (74 neutrons, 55 protons) or the features of the neutron states from  $^{129}\text{Xe}$  data (75 neutrons, 54 protons). In both neighboring nuclei, the magnetic moment (that is  $g$  factor) in the  $h_{11/2}$  as well as in  $s_{1/2}$  states has been measured [17]. The measured magnetic moments of these specified states allow, by using Eq. (9), to get the experimental values of the spin gyromagnetic factor  $g^s$  associated with odd proton and odd neutron. The obtained theoretical and experimental  $g^s$  values for proton and neutron are summarized in Table II and are used in further calculations for other orbitals. The  $g^s$  values listed in Table II have been used to calculate  $g_p$  and  $g_n$  values for particle configurations possibly involved in the structure of the  $I = 9^+$  isomeric state. The obtained  $g_p$  and  $g_n$  values have then been used to calculate the expected  $g$  factor of the isomeric bandhead for  $\pi h_{11/2} \otimes \nu h_{11/2}^{-1}$  configuration, see Eq.(8). All those values are listed in Table II.

By taking the  $g_p$  and  $g_n$  from theoretical estimates for  $h_{11/2}$  orbitals in  $^{128}\text{Cs}$  one gets purely theoretical expectation of the  $g$ -factor value for the  $I = 9^+$  isomeric state. Another possibility is to take the  $g_p$  and  $g_n$  values from magnetic moments measured for  $h_{11/2}$  states in single-odd neighbors. Since the same orbitals are involved in  $\pi h_{11/2} \otimes \nu h_{11/2}^{-1}$  chiral configuration in  $^{128}\text{Cs}$

the expected  $g$ -factor value should have the best correspondence to  $g = 0.59(1)$  reported here. Finally one can use the  $g_p$  and  $g_n$  values taken from magnetic moments measured for  $s_{1/2}$  states in single-odd neighbors excluding the possible involvement of collective rotation on single particle  $g_p$  and  $g_n$  values estimation. The three discussed scenarios give three expectation values of the  $g$  factor around 0.51 for each tested particle configuration within the simplest two-component model where the core rotation is excluded.

The discrepancy of the  $g$ -factor value  $g = 0.51$  expected theoretically and the experimental value  $g = 0.59(1)$ , see Table II, shows that the total spin of the  $I = 9^+$  isomeric state cannot be built chiefly by two angular momentum vectors of the odd nucleons. Significant core rotation component needs to be present in order to drive the  $g$  factor from  $g = 0.51$  towards the experimental value  $g = 0.59(1)$ . Thus, in the following we introduce a 3-component model which is appropriate for chiral geometry analysis.

### V. CHIRAL GEOMETRY IN A THREE-COMPONENT MODEL OF THE $g$ FACTOR

In the chiral scenario the odd-odd  $^{128}\text{Cs}$  nucleus studied here is built of three components contributing to the total magnetic moment of the isomeric state: the even-even core, the odd proton, and the odd neutron with angular momentum vectors  $\mathbf{j}_R$ ,  $\mathbf{j}_p$ , and  $\mathbf{j}_n$  respectively.

For the sake of simplicity, we calculate first the  $g$ -factor value using an additivity formula for the nuclear magnetic moment generalized to the 3-component system. In such a system, the total angular momentum vector of an excited state  $\mathbf{J}$  is a sum of angular momentum vectors of the components, which in case of  $^{128}\text{Cs}$  nucleus are the angular momentum of odd proton  $\mathbf{j}_p$ , odd neutron hole  $\mathbf{j}_n$ , and even-even core  $\mathbf{j}_R$ ,

$$\mathbf{j}_p + \mathbf{j}_n + \mathbf{j}_R = \mathbf{J}. \quad (11)$$

Thus the magnetic moment of a 3-component system becomes

$$\begin{aligned} \mu &= gJ\mu_N = \langle JJ|gJ_Z|JJ\rangle\mu_N \\ &= \langle JJ|g_p j_{pZ} + g_n j_{nZ} + g_R j_{RZ}|JJ\rangle\mu_N, \end{aligned} \quad (12)$$

where  $J_Z$ ,  $j_{pZ}$ ,  $j_{nZ}$ , and  $j_{RZ}$  are the angular momentum projection operators on the quantization axis of the total spin, spin of the proton, neutron, and core, respectively. With the use of the generalized Landé formula [13], the above equation can be expressed by the scalar product operators  $\mathbf{j}_p \cdot \mathbf{J}$ ,  $\mathbf{j}_n \cdot \mathbf{J}$ , and  $\mathbf{j}_R \cdot \mathbf{J}$ ,

$$\begin{aligned} \mu &= \frac{\langle JJ|g_p \mathbf{j}_p \cdot \mathbf{J} + g_n \mathbf{j}_n \cdot \mathbf{J} + g_R \mathbf{j}_R \cdot \mathbf{J}|JJ\rangle}{J(J+1)} \\ &\times \langle JJ|J_Z|JJ\rangle\mu_N. \end{aligned} \quad (13)$$

The  $g$  factor is thus given by the following formula

$$g = \frac{\langle JJ|g_p \mathbf{j}_p \cdot \mathbf{J} + g_n \mathbf{j}_n \cdot \mathbf{J} + g_R \mathbf{j}_R \cdot \mathbf{J}|JJ\rangle}{J(J+1)}. \quad (14)$$

By using the relation

$$J^2 = j_p^2 + j_n^2 + j_R^2 + 2\mathbf{j}_p \cdot \mathbf{j}_n + 2\mathbf{j}_p \cdot \mathbf{j}_R + 2\mathbf{j}_n \cdot \mathbf{j}_R, \quad (15)$$

one can write the final form of the  $g$ -factor expression, where only the scalar product operators of components are used,

$$\begin{aligned} g &= \frac{1}{2}(g_p + g_n + g_R) \\ &+ \frac{1}{J(J+1)} \cdot \frac{1}{2}j_p(j_p+1)(g_p - g_n - g_R) \\ &+ \frac{1}{J(J+1)} \cdot \frac{1}{2}j_n(j_n+1)(g_n - g_p - g_R) \\ &+ \frac{1}{J(J+1)} \cdot \frac{1}{2}j_R(j_R+1)(g_R - g_p - g_n) \\ &- \frac{1}{J(J+1)} (g_p \langle \mathbf{j}_n \cdot \mathbf{j}_R \rangle + g_n \langle \mathbf{j}_p \cdot \mathbf{j}_R \rangle + g_R \langle \mathbf{j}_p \cdot \mathbf{j}_n \rangle). \end{aligned} \quad (16)$$

Comparing the above generalized equation with the one derived from the coupling of only two angular momentum vectors (the additivity formula (7)), one can see that apart of the combinations of  $j_p^2$ ,  $j_n^2$ , and  $j_R^2$  quantities related to lengths of angular momentum vectors, an additional part that contains scalar products of the angular momentum vector pairs has appeared and thus is sensitive on their mutual orientation. The occurrence of this part has a geometrical physical explanation.

In case of the coupling of only two angular momentum vectors, the value of the total spin determines unambiguously their mutual orientation and the resulting magnetic moment. This does not hold for the coupling of three angular momentum vectors, where the same value of the total spin  $J$  can be attained at different angles between each pair of them giving different  $g$  factors. The last part of Eq. (16) vanishes for the ideal chiral geometry with all the vectors being mutually perpendicular, therefore the first four parts correspond to the  $g$ -factor value with maximum chirality  $g_{\text{chiral}}$  and Eq. (16) takes the simple form

$$\begin{aligned} g &= g_{\text{chiral}} \\ &- \frac{1}{J(J+1)} (g_p \langle \mathbf{j}_n \cdot \mathbf{j}_R \rangle + g_n \langle \mathbf{j}_p \cdot \mathbf{j}_R \rangle + g_R \langle \mathbf{j}_p \cdot \mathbf{j}_n \rangle). \end{aligned} \quad (17)$$

Semiclassical sequential coupling of the three angular momentum vectors explains the dependence of the  $g$ -factor value on their mutual angles.

Fig. 8 shows the angular momentum of the proton  $j_p$  and of the neutron  $j_n$  coupled to their resultant spin  $j_{pn}$ . The angular momentum of the core  $j_R$  may then be coupled to the  $j_{pn}$  at various precession angles to get the

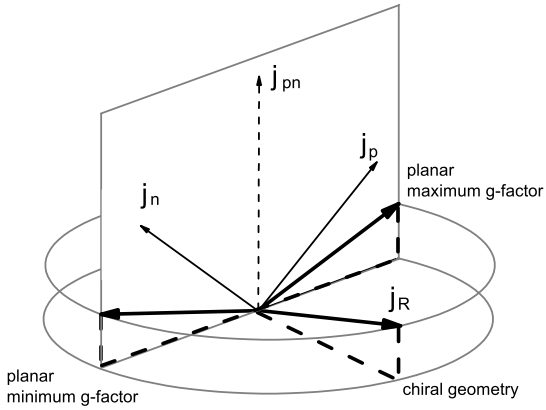


Figure 8: Core angular momentum  $\mathbf{j}_R$  may be coupled at different precession angles about the resultant  $\mathbf{j}_{pn}$  of proton and neutron angular momentum to form the specified spin of the isomeric state. The planar geometry where  $\mathbf{j}_R$  tends toward  $\mathbf{j}_p$  gives the highest possible value of the  $g$  factor. Second planar geometry where  $\mathbf{j}_R$  tends toward  $\mathbf{j}_n$  gives the lowest possible value of the  $g$  factor. Aplanar geometry corresponding to chiral configuration gives the  $g$ -factor value in between.

desired total spin  $J$ . In general, there are three characteristic cases given by this precession degree of freedom. The first case is the maximum aplanarity of the three angular momentum vectors, where the  $j_R$  vector goes as far as possible off the plane spanned by  $j_p$  and  $j_n$  giving a  $g$ -factor value corresponding to the maximum chirality. In the ideal chiral geometry, the  $g$  factor takes the value  $g_{\text{chiral}}$ . Next characteristic case is the planar geometry, where the angle between  $j_R$  and  $j_p$  attains a minimum value while the angle between  $j_R$  and  $j_n$  is the highest. Then, the scalar product  $\mathbf{j}_p \cdot \mathbf{j}_R$  has its maximum and the  $\mathbf{j}_n \cdot \mathbf{j}_R$  product its minimum. These scalar products are multiplied in Eq. (16) by  $g_n$  and  $g_p$  factors of opposite sign. Thus, in this scenario the part sensitive to the orientation of the three angular momentum vectors becomes maximally positive giving the highest  $g$ -factor value. The last characteristic case is an opposite planar geometry where  $j_R$  and  $j_n$  vectors become closest and the angle between  $j_R$  and  $j_p$  is highest leading to the maximum negative value of the part sensitive to angular momentum vectors geometry in Eq. (16). Such a geometry leads to the lowest value of the  $g$  factor. The two planar cases determine the limits of possible  $g$ -factor values for a given  $j_p$  and  $j_n$  coupling.

By making a plot of possible  $g$ -factor values versus the angle between proton and neutron angular momentum vectors one gets a drop-like shape containing all possible coupling schemes of the three components  $j_p$ ,  $j_n$ , and  $j_R$  to the total spin  $J$ . Fig. 9 shows two such plots for the coupling of  $\pi h_{11/2} \otimes \nu h_{11/2}^{-1}$  configuration with two main non-zero core angular momentum values  $j_R = 2\hbar$  and

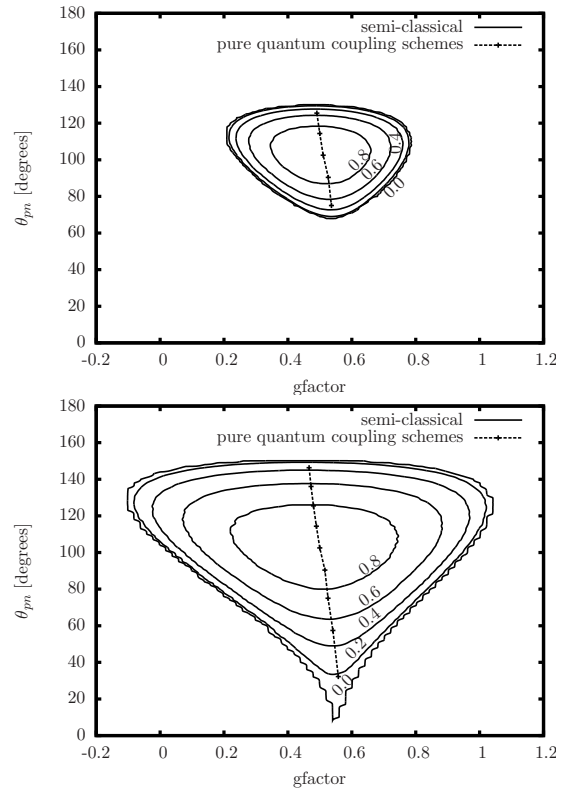


Figure 9: The  $g$ -factor value expected for coupling of  $\pi h_{11/2} \otimes \nu h_{11/2}^{-1}$  and core angular momentum  $j_R = 2\hbar$  (upper panel) and  $j_R = 4\hbar$  (lower panel) to the total spin  $I = 9\hbar$  of the isomeric state. Experimental values of  $g_p$  and  $g_n$  estimated from  $h_{11/2}$  orbital in single-odd neighboring nuclei have been used.

$j_R = 4\hbar$  to the total spin  $I = 9\hbar$  of the isomeric state. Contours shown in the plots present the absolute value of the normalized orientation parameter [18]

$$o = \frac{(\mathbf{j}_p \times \mathbf{j}_n) \cdot \mathbf{j}_R}{|\mathbf{j}_p| |\mathbf{j}_n| |\mathbf{j}_R|}, \quad (18)$$

calculated for each coupling scheme inside of the drop-like shape. The values of this parameter which are close to the zero correspond to planar  $|P\rangle$  configuration where all three angular momentum are in one plane. One can see that the planar configuration gives the outer border of the plot. In opposite, the values located in the middle of the plot which are close to unity correspond to the ideal chiral configurations  $|L\rangle$  and  $|R\rangle$ , where the three spins are perpendicular to each other.

According to Ref. [19], the existence of the chiral critical frequency would result in the planar orientation of the three angular momentum vectors for the  $I = 9\hbar$  isomeric bandhead. From the two opposite planar geometries, the one with proton angular momentum  $j_p$  tending towards the momentum of the core  $j_R$  is energy favored by Coriolis interaction. Therefore, the expected planar geometry should have the highest  $g$ -factor value for a given angle

$\theta_{pn}$  between  $j_p$  and  $j_n$ . This may lead to the  $g$ -factor values  $g \approx 0.5$ ,  $g \approx 0.7$ , and  $g \approx 0.9$  for the proton and the neutron coupled to the core state with  $j_R = 0\hbar$  (2-component model),  $j_R = 2\hbar$ , and  $j_R = 4\hbar$  (3-component model), respectively. The wave function of the isomeric state is a composition of several core rotational states. Contributions of  $j_R = 2\hbar$ ,  $j_R = 4\hbar$ , and higher (not discussed here) core rotations may drive the  $g$  factor from  $g = 0.51$  expected for  $j_R = 0\hbar$  to the experimental value  $g = 0.59(1)$  provided planar geometry in the isomeric bandhead.

The above analysis shows that the two-component model where the total spin of the isomeric state is built chiefly by the angular momentum vectors of the two odd nucleons cannot reproduce the experimental  $g$ -factor value. The composition of the wave function with the non-zero core rotation (the three-component model) is needed to reproduce the measured  $g$  factor within pure  $\pi h_{11/2} \otimes \nu h_{11/2}^{-1}$  configuration where a non-chiral geometry of the isomeric bandhead is expected. The wave function composition is discussed in a quantum-mechanical approach in the following sections.

## VI. QUANTUM MECHANICAL CALCULATION OF THE $g$ FACTOR OF THREE-BODY SYSTEM

In the semi-classical models discussed above, the angular momentum vectors  $\mathbf{j}$  were taken as classical vectors with three spatial components well defined and the length  $j(j+1)$ . Except triangularity, these models do not impose any condition on the mutual angles between these

three coupled vectors. In general, the idea of the nuclear chirality requires that all three spatial components of the coupled spins are well defined, which seems to contradict with quantum approach, where only the length and the projection on the quantization axis are defined for an angular momentum vector. It is therefore essential to begin with principles of the chiral geometry emerging in quantum systems.

The nuclear state of a definite spin,  $|JM\rangle$  can be expressed as a product of the states of proton  $|j_p\rangle$ , neutron  $|j_n\rangle$ , and core  $|j_R\rangle$ , respectively, coupled to the total angular momentum as follows:  $\mathbf{j}_p, \mathbf{j}_n$  coupled to a vector  $\mathbf{j}_{pn} = \mathbf{j}_p + \mathbf{j}_n$  which, in turn, is coupled with  $\mathbf{j}_R$  to  $\mathbf{J} = \mathbf{j}_{pn} + \mathbf{j}_R$ ,

$$\begin{aligned} & |(j_p j_n) j_{pn} j_R; JM\rangle \\ &= \sum_{m_p, m_n, m_{pn}, m_R} \langle j_p m_p j_n m_n | j_{pn} m_{pn} \rangle \\ & \times \langle j_{pn} m_{pn} j_R m_R | JM \rangle |j_p m_p\rangle |j_n m_n\rangle |j_R m_R\rangle. \end{aligned} \quad (19)$$

There are several possible  $j_{pn}$  quantum numbers indicating that the total spin state  $|JM\rangle$  may be formed in several ways, here called coupling schemes. A single coupling scheme given by Eq. (19) defines a unique set of expected mutual angles between each pair of the angular momentum vectors. For the total spin state  $|JM\rangle$  resulting from a single coupling scheme, its  $g$  factor can be calculated analytically using angular momentum algebra. The matrix elements of the squares and scalar products in Eq. (16) for a single coupling scheme are given by

$$\langle (j'_p j'_n) j'_{pn} j'_R; J' M' | \mathbf{j}_p^2 | (j_p j_n) j_{pn} j_R; JM \rangle = \delta_{J'J} \delta_{M'M} \delta_{j'_p j_p} \delta_{j'_n j_n} \delta_{j'_R j_R} \delta_{j'_{pn} j_{pn}} j_p (j_p + 1), \quad (20)$$

$$\langle (j'_p j'_n) j'_{pn} j'_R; J' M' | \mathbf{j}_n^2 | (j_p j_n) j_{pn} j_R; JM \rangle = \delta_{J'J} \delta_{M'M} \delta_{j'_p j_p} \delta_{j'_n j_n} \delta_{j'_R j_R} \delta_{j'_{pn} j_{pn}} j_n (j_n + 1), \quad (21)$$

$$\langle (j'_p j'_n) j'_{pn} j'_R; J' M' | \mathbf{j}_R^2 | (j_p j_n) j_{pn} j_R; JM \rangle = \delta_{J'J} \delta_{M'M} \delta_{j'_p j_p} \delta_{j'_n j_n} \delta_{j'_R j_R} \delta_{j'_{pn} j_{pn}} j_R (j_R + 1), \quad (22)$$

$$\begin{aligned} & \langle (j'_p j'_n) j'_{pn} j'_R; J' M' | \mathbf{j}_p \cdot \mathbf{j}_n | (j_p j_n) j_{pn} j_R; JM \rangle = \delta_{J'J} \delta_{M'M} \delta_{j'_p j_p} \delta_{j'_n j_n} \delta_{j'_R j_R} \delta_{j'_{pn} j_{pn}} (-1)^{j_p + j_n + j_{pn}} \\ & \times \sqrt{j_p(j_p + 1)(2j_p + 1)j_n(j_n + 1)(2j_n + 1)} \begin{Bmatrix} j_p & j_n & j_{pn} \\ j_n & j_p & 1 \end{Bmatrix}, \end{aligned} \quad (23)$$

$$\begin{aligned} & \langle (j'_p j'_n) j'_{pn} j'_R; J' M' | \mathbf{j}_p \cdot \mathbf{j}_R | (j_p j_n) j_{pn} j_R; JM \rangle = \delta_{J'J} \delta_{M'M} \delta_{j'_p j_p} \delta_{j'_n j_n} \delta_{j'_R j_R} (-1)^{j_R + j_p + j_n + J + 1} \\ & \times \sqrt{(2j_{pn} + 1)(2j'_{pn} + 1)} \sqrt{j_p(j_p + 1)(2j_p + 1)} \sqrt{j_R(j_R + 1)(2j_R + 1)} \\ & \times \begin{Bmatrix} j_p & j_{pn} & j_n \\ j'_{pn} & j_p & 1 \end{Bmatrix} \begin{Bmatrix} j_{pn} & j_R & J \\ j_R & j'_{pn} & 1 \end{Bmatrix}, \end{aligned} \quad (24)$$

$$\begin{aligned} & \langle (j'_p j'_n) j'_{pn} j'_R; J' M' | \mathbf{j}_n \cdot \mathbf{j}_R | (j_p j_n) j_{pn} j_R; JM \rangle = \delta_{J'J} \delta_{M'M} \delta_{j'_p j_p} \delta_{j'_n j_n} \delta_{j'_R j_R} (-1)^{j_R + j_p + j_n + J + 1 + j_{pn} + j'_{pn}} \\ & \times \sqrt{(2j_{pn} + 1)(2j'_{pn} + 1)} \sqrt{j_n(j_n + 1)(2j_n + 1)} \sqrt{j_R(j_R + 1)(2j_R + 1)} \\ & \times \begin{Bmatrix} j_n & j_{pn} & j_p \\ j'_{pn} & j_n & 1 \end{Bmatrix} \begin{Bmatrix} j_{pn} & j_R & J \\ j_R & j'_{pn} & 1 \end{Bmatrix}, \end{aligned} \quad (25)$$

where non-zero values of the six- $j$  symbols give all possible

coupling schemes. One can calculate the set of the  $g$ -

factor values corresponding to possible coupling schemes by substituting the matrix elements (20)-(25) together with the values of  $g_p$ ,  $g_n$ , and  $g_R$  into Eq. (16). Two such sets, one for  $j_R = 2\hbar$  and one for  $j_R = 4\hbar$ , are presented in Fig.9 as small crosses connected with dotted lines. This analytical approach shows that the idea of the nuclear chirality, with three well defined angles between the pairs of three spins does not contradict to the quantum angular momentum algebra.

In general, the state with definite spin  $|JM\rangle$  is a superposition of many coupling schemes (only the angular

momentum quantum numbers are exposed)

$$|JM\rangle = \sum_{j_p, j_n, j_{pn}, j_R} c_J(j_p, j_n, j_{pn}, j_R) |(j_p j_n) j_{pn} j_R; JM\rangle. \quad (26)$$

Then, the geometry defined by the mean values of the squares and scalar products of the three angular momentum vectors is also given by the superposition coefficients  $c_J(j_p, j_n, j_{pn}, j_R)$ . Indeed, the expectation values in question takes for the wave packet the following form

$$\langle JM | \mathbf{j}_p^2 | JM \rangle = \sum_{j_p, j_n, j_{pn}, j_R} |c_J(j_p, j_n, j_{pn}, j_R)|^2 j_p(j_p + 1), \quad (27)$$

$$\langle JM | \mathbf{j}_n^2 | JM \rangle = \sum_{j_p, j_n, j_{pn}, j_R} |c_J(j_p, j_n, j_{pn}, j_R)|^2 j_n(j_n + 1), \quad (28)$$

$$\langle JM | \mathbf{j}_R^2 | JM \rangle = \sum_{j_p, j_n, j_{pn}, j_R} |c_J(j_p, j_n, j_{pn}, j_R)|^2 j_R(j_R + 1), \quad (29)$$

$$\begin{aligned} \langle JM | \mathbf{j}_p \cdot \mathbf{j}_n | JM \rangle &= \sum_{j_p, j_n, j_{pn}, j_R} |c_J(j_p, j_n, j_{pn}, j_R)|^2 \\ &\times \langle (j_p j_n) j_{pn} j_R; JM | \mathbf{j}_p \cdot \mathbf{j}_n | (j_p j_n) j_{pn} j_R; JM \rangle, \end{aligned} \quad (30)$$

$$\begin{aligned} \langle JM | \mathbf{j}_p \cdot \mathbf{j}_R | JM \rangle &= \sum_{j_p, j_n, j_{pn}, j'_R} c_J^*(j_p, j_n, j_{pn}, j_R) c_J(j_p, j_n, j_{pn}, j'_R) \\ &\times \langle (j_p j_n) j'_{pn} j_R; JM | \mathbf{j}_p \cdot \mathbf{j}_R | (j_p j_n) j_{pn} j_R; JM \rangle, \end{aligned} \quad (31)$$

$$\begin{aligned} \langle JM | \mathbf{j}_n \cdot \mathbf{j}_R | JM \rangle &= \sum_{j_p, j_n, j_{pn}, j'_R} c_J^*(j_p, j_n, j_{pn}, j_R) c_J(j_p, j_n, j_{pn}, j'_R) \\ &\times \langle (j_p j_n) j'_{pn} j_R; JM | \mathbf{j}_n \cdot \mathbf{j}_R | (j_p j_n) j_{pn} j_R; JM \rangle. \end{aligned} \quad (32)$$

Such superpositions can be analyzed with available nuclear models which give the superposition coefficients  $c_J(j_p, j_n, j_{pn}, j_R)$ .

## VII. PARTICLE ROTOR MODEL CALCULATIONS

In the present section, the  $g$  factor is calculated in the framework of the triaxial particle rotor model (PRM), whose formalism in detail can be found in Refs. [1, 20–27].

In the present work, a many-particle-many-hole PRM [22, 23] is used. The total Hamiltonian of PRM is expressed as

$$\hat{H}_{\text{PRM}} = \hat{H}_{\text{coll}} + \hat{H}_{\text{intr}}, \quad (33)$$

with the collective rotor Hamiltonian

$$\hat{H}_{\text{coll}} = \sum_{k=1}^3 \frac{\hat{j}_{Rk}^2}{2\mathcal{J}_k} = \sum_{k=1}^3 \frac{(\hat{J}_k - \hat{j}_{pk} - \hat{j}_{nk})^2}{2\mathcal{J}_k}, \quad (34)$$

where the indices  $k = 1, 2$ , and  $3$  refer to the three principal axes of the body-fixed frame. The  $\hat{j}_{Rk}$  and  $\hat{J}_k$  denote the angular momentum operators of the core and of the total nucleus, respectively, and the  $\hat{j}_{pk}$  and  $\hat{j}_{nk}$  the angular momentum operator of the valence protons and neutrons. The moments of inertia of the irrotational flow type are adopted, i.e.,  $\mathcal{J}_k = \mathcal{J}_0 \sin^2(\gamma - 2k\pi/3)$ , with  $\gamma$  the triaxial deformation parameter. In addition, the intrinsic Hamiltonian is written as

$$H_{\text{intr}} = \sum_{i=p,n} \sum_{\nu} \varepsilon_{i,\nu} a_{i,\nu}^{\dagger} a_{i,\nu}, \quad (35)$$

where  $\varepsilon_{p,\nu}$  and  $\varepsilon_{n,\nu}$  are the single particle energies provided by single- $j$  shell

$$h_{\text{sp}} = \pm \frac{1}{2} C \left\{ \cos \gamma \left( j_3^2 - \frac{j(j+1)}{3} \right) + \frac{\sin \gamma}{2\sqrt{3}} (j_+^2 + j_-^2) \right\}. \quad (36)$$

Here, the plus or minus sign refers to particle or hole, and the coefficient  $C$  is proportional to the quadrupole

deformation  $\beta$  [28]

$$C = \left( \frac{123}{8} \sqrt{\frac{5}{\pi}} \right) \frac{2N+3}{j(j+1)} A^{-1/3} \beta. \quad (37)$$

The single particle state and its time reversal state are expressed as

$$a_{\nu}^{\dagger}|0\rangle = \sum_{\alpha\Omega} c_{\alpha\Omega}^{\nu} |\alpha, j\Omega\rangle, \quad (38)$$

$$a_{\bar{\nu}}^{\dagger}|0\rangle = \sum_{\alpha\Omega} (-1)^{j-\Omega} c_{\alpha\Omega}^{\nu} |\alpha, j-\Omega\rangle, \quad (39)$$

where  $\Omega$  is the projection of the single-particle angular momentum  $j$  along the 3-axis of the intrinsic frame and restricted to  $\dots, -3/2, 1/2, 5/2, \dots$  due to the time-reversal degeneracy, and  $\alpha$  denotes the other quantum numbers. For a system with  $\sum_{i=p,n} N_i$  valence nucleons ( $N_i$  denotes the number of the protons or neutrons in the valence shell), the intrinsic wave function is given as

$$|\varphi\rangle = \prod_{i=p,n} \left( \prod_{l=1}^{n_i} a_{i,\nu_l}^{\dagger} \right) \left( \prod_{l=1}^{n'_i} a_{i,\bar{\nu}_l}^{\dagger} \right) |0\rangle, \quad (40)$$

with  $n_i + n'_i = N_i$  and  $0 \leq n_i \leq N_i$ .

The total wave function can be expanded into the strong coupling basis

$$|JM\rangle = \sum_{K\varphi} c_{K\varphi} |JMK\varphi\rangle, \quad (41)$$

with

$$|JMK\varphi\rangle = \frac{1}{\sqrt{2(1+\delta_{K0}\delta_{\varphi,\bar{\varphi}})}} (|JMK\rangle|\varphi\rangle + (-1)^{I-K} |JM-K\rangle|\bar{\varphi}\rangle), \quad (42)$$

where  $|JMK\rangle$  is the Wigner function  $\sqrt{\frac{2J+1}{8\pi^2}} D_{MK}^J$ . The basis states are symmetrized under the point group  $D_2$ , which leads to  $K - \frac{1}{2} \sum_{i=1}^4 (n_i - n'_i)$  being an even integer.

After obtaining the wave functions of PRM, the reduced transition probabilities  $B(M1)$  and  $B(E2)$ , and the expectation values of the angular momentum of the system can be calculated [22, 23]. For the  $g$ -factor calculation, one uses Eq. (14) [8, 25, 26].

In the PRM calculation, the configuration  $\pi h_{11/2} \otimes \nu h_{11/2}^{-5}$  with the corresponding deformation parameters  $\beta = 0.23$  and  $\gamma = 24^\circ$ , according to the adiabatic and configuration-fixed constrained covariant density functional theory (CDFT) calculations [8, 29], are used with the PC-PK1 density functional [30]. The moment of inertia  $\mathcal{J}_0 = 20 \hbar^2/\text{MeV}$  is adjusted to fit the energy spectra of yrast band. For the electromagnetic transitions, the empirical intrinsic quadrupole moment  $Q_0 = (3/\sqrt{5\pi}) R_0^2 Z\beta$ , and the  $g$  factors of proton  $g_p$  and neutron  $g_n$  given in Table II<sup>a</sup> have been adopted along with the core  $g$ -factor value  $g_R = 0.41$  taken from  $^{128}\text{Xe}$  2<sup>+</sup> experimental data [31].

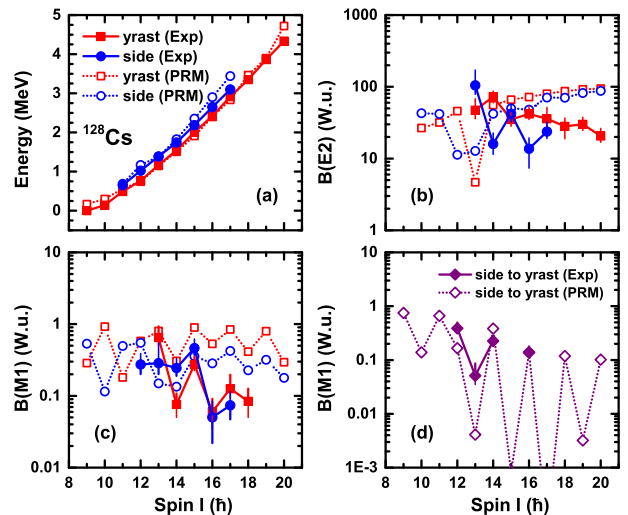


Figure 10: (a) The energy spectra, (b) the intraband  $B(E2)$ , (c) the intraband  $B(M1)$ , and (d) the interband  $B(M1)$  of the doublet bands in  $^{128}\text{Cs}$  calculated by the PRM approach in comparison with the experimental data available [3].

In Fig. 10, the energy spectra, the intraband  $B(E2)$  and  $B(M1)$ , and the interband  $B(M1)$  of the doublet bands in  $^{128}\text{Cs}$  calculated by PRM in comparison with the experimental data available [3] are shown. The observed energy spectra are reproduced well as shown in Fig. 10(a), including the energy difference between the partner bands. The trend of the calculated  $B(E2)$  results deviates from the data due to the frozen nuclear shape. The staggering of the intraband and the interband  $B(M1)$  can be seen in both the data and the calculated results as shown in Figs. 10(c) and 10(d). Their strengths are reproduced reasonably. All of these agreements support the correct assignment for the valence nucleon configuration.

The  $g$  factor is sensitive to the configuration and the triaxial deformation parameter. To further check the configuration assignment, we display in Fig. 11 the  $g$ -factor values for 9<sup>+</sup> yrast bandhead as a function of triaxial deformation calculated by PRM with configurations  $\pi h_{11/2} \otimes \nu h_{11/2}^{-5}$ ,  $\pi h_{11/2} \otimes \nu h_{11/2}^{-3}$ , and  $\pi h_{11/2} \otimes \nu h_{11/2}^{-1}$ . In these calculations, the triaxial deformation parameter is varied. For the neutron configuration,  $-5$  denotes that there are five holes located in the  $h_{11/2}$  shell and four of them are paired. One notices that if the triaxial deformation parameter is equal to that obtained from the constrained CDFT calculations, the calculated  $g$  factor with the configuration  $\pi h_{11/2} \otimes \nu h_{11/2}^{-5}$ , which is also predicted by the constrained CDFT calculations, is closest to the experimental value.

By keeping the quadrupole deformation and decreasing the parameter  $\gamma \rightarrow 0^\circ$  the nuclear shape becomes axially symmetric with prolate deformation. This is the second characteristic case of the nuclear orientation as discussed above, i.e., planar geometry with the angle be-

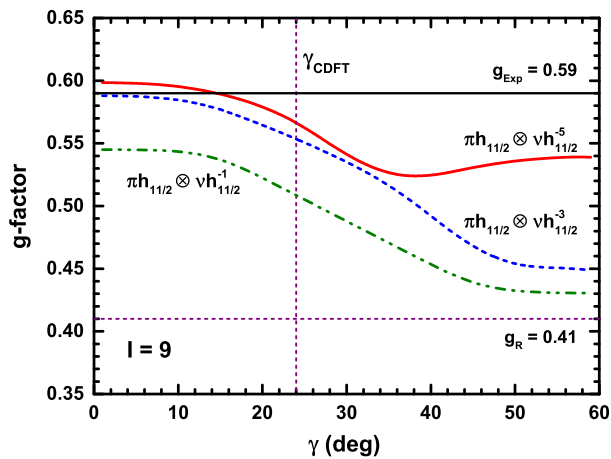


Figure 11: The  $g$ -factor values for  $9^+$  yrast bandhead as a function of triaxial deformation calculated by PRM with configurations  $\pi h_{11/2} \otimes \nu h_{11/2}^{-5}$ ,  $\pi h_{11/2} \otimes \nu h_{11/2}^{-3}$ , and  $\pi h_{11/2} \otimes \nu h_{11/2}^{-1}$ .

tween  $j_R$  and  $j_p$  attaining a minimum value while the angle between  $j_R$  and  $j_n$  being the highest, and gives the highest  $g$ -factor value. The non-chiral  $g$ -factor value obtained with axially symmetric core for configurations  $\pi h_{11/2} \otimes \nu h_{11/2}^{-5}$  ( $g \approx 0.60$ ) and  $\pi h_{11/2} \otimes \nu h_{11/2}^{-3}$  ( $g \approx 0.59$ ) agree very well with the experimental  $g$  factor  $g=0.59(1)$ . When increasing the parameter  $\gamma \rightarrow 60^\circ$ , the nuclear shape becomes oblately deformed. For the configurations  $\pi h_{11/2} \otimes \nu h_{11/2}^{-3}$  and  $\pi h_{11/2} \otimes \nu h_{11/2}^{-1}$ , the neutron angular momentum  $j_n$  aligns mainly along the long-axis and becomes closed to the  $j_R$ , while the angle between  $j_R$  and  $j_p$  is highest. This is the third characteristic case of the nuclear orientation and leads to the lowest  $g$ -factor value. For the configuration  $\pi h_{11/2} \otimes \nu h_{11/2}^{-5}$  with lower neutron Fermi surface, the situation become complicated. The lowest  $g$ -factor value does not appear at  $\gamma \approx 60^\circ$ , but  $\gamma \approx 38^\circ$ . This might be due to the neutron angular momentum has large intermediate axis component at  $\gamma \approx 38^\circ$  and becomes close to the core angular momentum  $j_R$ .

Fig. 12 presents  $g$ -factor values as functions of spin expected for  $\pi h_{11/2} \otimes \nu h_{11/2}^{-5}$  yrast band levels with triaxial deformation parameters  $\gamma = 0^\circ$  (axial symmetric limit),  $24^\circ$  (obtained from constrained CDFT),  $30^\circ$  (maximal asymmetric deformation), and  $38^\circ$  (gives lowest  $g$ -factor value at bandhead) in comparison with the available experimental data. For the triaxially deformed core  $\gamma = 24^\circ$  the  $g$ -factor value  $g = 0.57$  is obtained for the calculated  $9^+$  bandhead. This value decreases with spin and reaches  $g \approx 0.42$  for spin  $I = 20\hbar$ .

One can see in Fig. 12 that the  $g$  factor of the yrast states for the triaxial shapes of the nucleus are systematically smaller than the corresponding values for the axial deformation  $\gamma = 0^\circ$ . It indicates that the geometry of the three angular momentum vectors evolves from the planar

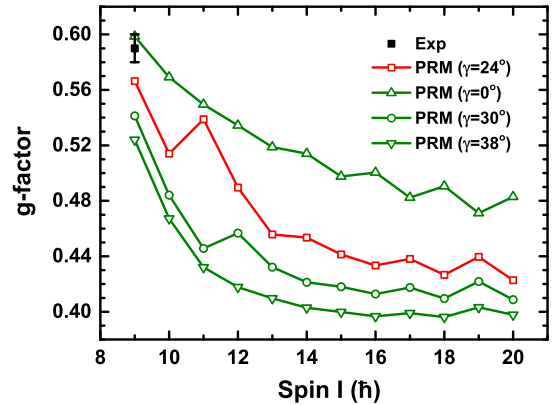


Figure 12: The  $g$ -factor values as functions of spin expected for  $\pi h_{11/2} \otimes \nu h_{11/2}^{-5}$  yrast band levels with triaxial deformation parameters  $\gamma = 0^\circ, 24^\circ, 30^\circ$ , and  $38^\circ$ .

limit toward the chiral one.

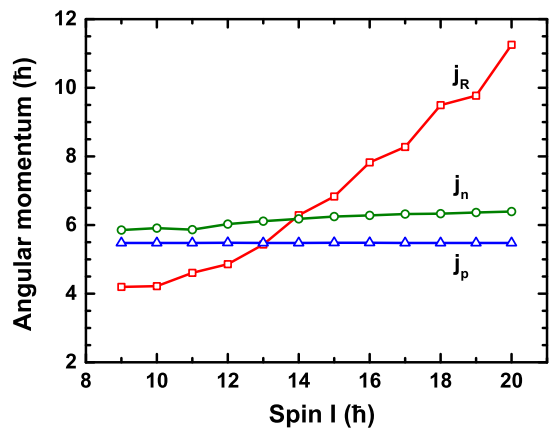


Figure 13: The absolute values of angular momentum of proton  $j_p$ , neutron  $j_n$ , and core  $j_R$  as functions of spin expected for  $\pi h_{11/2} \otimes \nu h_{11/2}^{-5}$  yrast band levels with triaxial deformation parameters  $\gamma = 24^\circ$ .

As mentioned above, a 2-component model without including the core angular momentum contribution gives large discrepancy in comparison with the experimental data. To check this in the framework of PRM, we plot in Fig. 13 the absolute values of angular momentum of core  $j_R$  together with proton  $j_p$  and neutron  $j_n$  as functions of spin for  $\pi h_{11/2} \otimes \nu h_{11/2}^{-5}$  yrast band levels with the triaxial deformation parameter  $\gamma = 24^\circ$ . In the calculations, a quantal correction  $1/2$  has been taken into account, i.e.,

$$j = \sqrt{\langle j_1^2 \rangle + \langle j_2^2 \rangle + \langle j_3^2 \rangle} - 1/2. \quad (43)$$

Note that the proton angular momentum is a good quantum number, while the angular momentum of five neutron holes and core are not. One can see that  $j_n$  does not change much with increasing spin. However,  $j_R$  increases

from  $j_R \approx 4.2\hbar$  at  $I = 9\hbar$  to  $j_R \approx 11.3\hbar$  at  $I = 20\hbar$ , which indicates that the angular momentum of the rotor plays gradually more important roles than those of the proton particle and neutron holes. Thus, although the rotor angular momentum at the bandhead of  $^{128}\text{Cs}$  yrast band is smaller than those of proton and neutron, it cannot be overlooked.

### VIII. SUMMARY

Spontaneous chiral symmetry breaking in the  $^{128}\text{Cs}$  nucleus has been previously reported through observation of two nearly degenerated rotational bands with specific selection rules of the gamma transitions. These features have been observed for significant nuclear rotation corresponding to  $I > 13\hbar$  of the excited states. For lower spins the rotational band which is partner to the yrast band is not seen experimentally suggesting the existence of the critical frequency of the chiral rotation. Below the critical frequency the chiral geometry of the three angular momentum vectors is prevented possibly canceling the degeneration of the yrast and yrare bands. The hypothesis of the critical frequency has been explored through  $g$ -factor measurement of the yrast band-

head within TDAPD method. The experimental results have been discussed in frame of quantum angular momentum algebra, semi-classical calculations, and in the framework of PRM.

The experimental  $g$ -factor value of the isomeric  $I = 9^+$  bandhead of the yrast states is well reproduced by PRM with the planar geometry of the three spins obtained in the limit of axially symmetric deformation. This result may explain the absence of the low spin yrare states and is the first indication of the existence of the chiral critical frequency.

### IX. ACKNOWLEDGMENTS

The authors wish to thank the ORSAY Tandem team for providing an excellent and stable beam. This project was supported in part by Polish National Science Centre (NCN), grant No 2013/10/M/ST2/00427. This work was partially supported by the Polish-French Collaboration COPIN-IN2P3 (06-121). This work was partly supported by the National Key R&D Program of China (Contracts No. 2018YFA0404400 and 2017YFE0116700), the National Natural Science Foundation of China (Grants No. 12070131001, 11875075, 11935003, and 11975031).

- 
- [1] S. Frauendorf and J. Meng, Nucl. Phys. A **617**, 131 (1997).
  - [2] T. Koike, K. Starosta, C. J. Chiara, D. B. Fossan, and D. R. LaFosse, Phys. Rev. C **67**, 044319 (2003).
  - [3] E. Grodner *et al.*, Phys. Rev. Lett **97**, 172501 (2006).
  - [4] T. Koike, K. Starosta, and I. Hamamoto, Phys. Rev. Lett. **93**, 172502 (2004).
  - [5] E. Grodner, I. Sankowska, T. Morek, S. G. Rohoziński, C. Droste, J. Srebrny, A. A. Pasternak, M. Kisieliński, M. Kowalczyk, J. Kownacki, et al., Phys. Lett. B **703**, 46 (2011).
  - [6] T. Marchlewski, R. Szenborn, J. Samorajczyk, E. Grodner, J. Srebrny, C. Droste, L. Próchniak, A. A. Pasternak, M. Kowalczyk, M. Kisieliński, et al., Acta Phys.Polon.B **46** (2015) 3, 689
  - [7] P. Olbratowski, J. Dobaczewski and J. Dudek, Phys. Rev. C **73**, 054308 (2006).
  - [8] E. Grodner et al., Phys. Rev. Lett. **120**, 022502 (2018).
  - [9] E. Grodner et al., *to be submitted to Phys. Rev. C*.
  - [10] Ch. Droste, S. G. Rohoziński, K. Starosta, L. Próchniak, and E. Grodner, Eur. Phys. J. A **42**, 79-89 (2009).
  - [11] S. G. Rohoziński, L. Próchniak, K. Starosta and Ch. Droste, Eur. Phys. J. A **47**, 90, (2011).
  - [12] N. J. Stone, At. Data Nucl. Data Tables 90, 75 (2005).
  - [13] P. J. Brussaard, *Shell-model and applications in nuclear spectroscopy*, North-Holland (1977).
  - [14] J. Meng (Ed), *Relativistic Density Functional for Nuclear Structure* World Scientific, Singapore, (2016).
  - [15] J.-M. Yao, J. Peng, J. Meng, and P. Ring, Sci. China Phys. Mech. Astron. **54**, 198 (2011).
  - [16] J. Li, J. X. Wei, J. N. Hu, P. Ring, and J. Meng, Phys. Rev. C **88**, 064307 (2013).
  - [17] P. Raghavan *Table of nuclear moments*. At. Data Nucl. Data Tables 42, 189 (1989).
  - [18] K.Starosta, T.Koike, C.J.Chiara, D.B.Fossan, and D.R.LaFosse, Nucl. Phys. A **682**, 375c (2001).
  - [19] P. Olbratowski, J. Dobaczewski, J. Dudek, W. Plóciennik, Phys. Rev. Lett. **93**, 052501 (2004).
  - [20] J. Peng, J. Meng, and S. Q. Zhang, Phys. Rev. C **68**, 044324 (2003).
  - [21] S. Q. Zhang, B. Qi, S. Y. Wang, J. Meng, Phys. Rev. C **75**, 044307 (2007).
  - [22] B. Qi, S. Q. Zhang, J. Meng, S. Y. Wang, S. Frauendorf, Phys. Lett. B **675**, 175 (2009).
  - [23] Q. B. Chen, B. F. Lv, C. M. Petrache, J. Meng, Phys. Lett. B **782**, 744 (2018).
  - [24] Q. B. Chen, N. Kaiser, Ulf-G. Meißner, J. Meng, Phys. Rev. C **99**, 064326 (2019).
  - [25] Q. B. Chen, N. Kaiser, Ulf-G. Meißner, and J. Meng, Phys. Lett. B **807**, 135568 (2020).
  - [26] Q. B. Chen, S. Frauendorf, N. Kaiser, Ulf-G. Meißner, J. Meng, Phys. Lett. B **807**, 135596 (2020).
  - [27] C. Broocks, Q. B. Chen, N. Kaiser, Ulf-G. Meißner, Eur. Phys. J. A **57**, 161 (2021).
  - [28] S. Y. Wang, B. Qi, and S. Q. Zhang, Chin. Phys. Lett. **26**, 052102 (2009).
  - [29] J. Meng, J. Peng, S. Q. Zhang, and S.-G. Zhou, Phys. Rev. C **73**, 037303 (2006).
  - [30] P. W. Zhao, Z. P. Li, J. M. Yao, and J. Meng, Phys. Rev. C **82**, 054319 (2010)
  - [31] A. Arnesen, K. Johansson, E. Karlsson, T. Noreland, L.-O. Norlin, and S. Ogaza, Hyperfine Interact. **5**, 81 (1977).